LETTER

Perovskite/Colloidal Quantum Dot Tandem Solar Cells: Theoretical Modeling and Monolithic Structure

Arfa Karani,[†,#] Le Yang,[†,‡,#] Sai Bai,[‖,⊥] Moritz H. Futscher,[§] Henry J. Snaith,[‖] Bruno Ehrler,[§] Neil C. Greenham,*[,†] and Dawei Di*[,†]

[†]Cavendish Laboratory, University of Cambridge, JJ Thomson Avenue, Cambridge CB3 0HE, United Kingdom

[‡]Institute of Materials Research and Engineering (IMRE), Agency for Science, Technology and Research (A*STAR), 2 Fusionopolis Way, Singapore 138634, Singapore

[‖]Clarendon Laboratory, Department of Physics, University of Oxford, Parks Road, Oxford OX1 3PU, United Kingdom

[⊥]Department of Physics, Chemistry and Biology (IFM), Linköping University, Linköping SE-581 83, Sweden

[§]Centre for Nanophotonics, AMOLF, Science Park 104, 1098XG Amsterdam, The Netherlands

ABSTRACT: Metal-halide perovskite-based tandem solar cells show great promise for overcoming the Shockley−Queisser single-junction efficiency limit via low-cost tandem structures, but so far, they employ conventional bottom-cell materials that require stringent processing conditions. Meanwhile, difficulty in achieving low-bandgap (<1.1 eV) perovskites limits all-perovskite tandem cell development. Here we propose a tandem cell design based on a halide perovskite top cell and a chalcogenide colloidal quantum dot (CQD) bottom cell, where both materials provide bandgap tunability and solution processability. A theoretical efficiency of 43% is calculated for tandem-cell bandgap combinations of 1.55 (perovskite) and 1.0 eV (CQDs) under 1-sun illumination. We highlight that intersubcell radiative coupling contributes significantly (>11% absolute gain) to the ultimate efficiency via photon recycling. We report an initial experimental demonstration of a solution-processed monolithic perovskite/CQD tandem solar cell, showing evidence for subcell voltage addition. We model that a power conversion efficiency of 29.7% is possible by combining state-of-the-art perovskite and CQD solar cells.
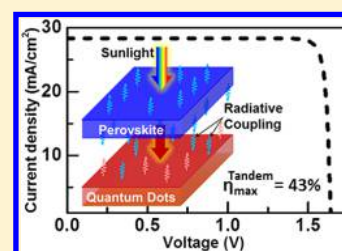
With significant cost reductions over the past decade, photovoltaic solar cells are now well positioned to provide one of the most economically affordable options for future energy generation. Improvements of solar cell power conversion efficiencies (PCEs) play a critical role in strengthening this position. The current photovoltaic industry is dominated by conventional single-junction silicon (Si) solar cells that exhibit practical efficiencies of up to ∼25%, and further efficiency enhancements are constrained by the Shockley−Queisser (SQ) limit of ∼30%.[1−3] The industry seeks alternatives to go beyond this threshold. One of the most effective ways to overcome this constraint is to use a tandem configuration formed by a series of subcells with descending bandgaps, so that photons from the solar spectrum with different energies can be selectively absorbed and converted by the subcells most efficiently. High-efficiency tandem solar cells with 1-sun efficiencies of up to ∼39% have been demonstrated.[4,5] However, these cells are based on III−V semiconductors manufactured by highly expensive processes such as epitaxy.[5,6] Producing efficient tandem cells using low-cost methods remains a challenge.[2,6]

With the steep increase of efficiencies in recent years, metal-halide perovskite solar cells have shown great potential to become a low-cost alternative to conventional photovoltaics.[2,7,8] While single-junction perovskite and perovskite/perovskite tandem cells have already been demonstrated,[9−11] it is important to note that the near-infrared (near-IR) photons are not effectively captured by such devices due to the limited bandgap tunability of the perovskite material family. Therefore, the best perovskite/perovskite and perovskite/organic tandem solar cells only utilize photons with wavelengths shorter than ∼1000 nm ($E_{photon} \gtrsim 1.24$ eV).[11−13] The stability issue of the tin-based perovskite used to obtain the low bandgap is yet to be overcome.[14−16] Similarly, the absorption edge of perovskite/Si tandem devices is limited to ∼1100 nm ($E_{photon} \gtrsim 1.12$ eV, the bandgap of Si).[17−19] Other solution-processed tandems such as organic/organic tandem devices can convert photons with wavelengths of less than ∼900 nm ($E_{photon} \gtrsim 1.37$ eV).[20,21] Due to the broad bandgap tunability of the chalcogenide colloidal quantum dots (CQDs) including lead sulfide (PbS) and lead selenide (PbSe),[22−25] they provide ideal bandgap matching with the perovskite top cells in a tandem structure and can
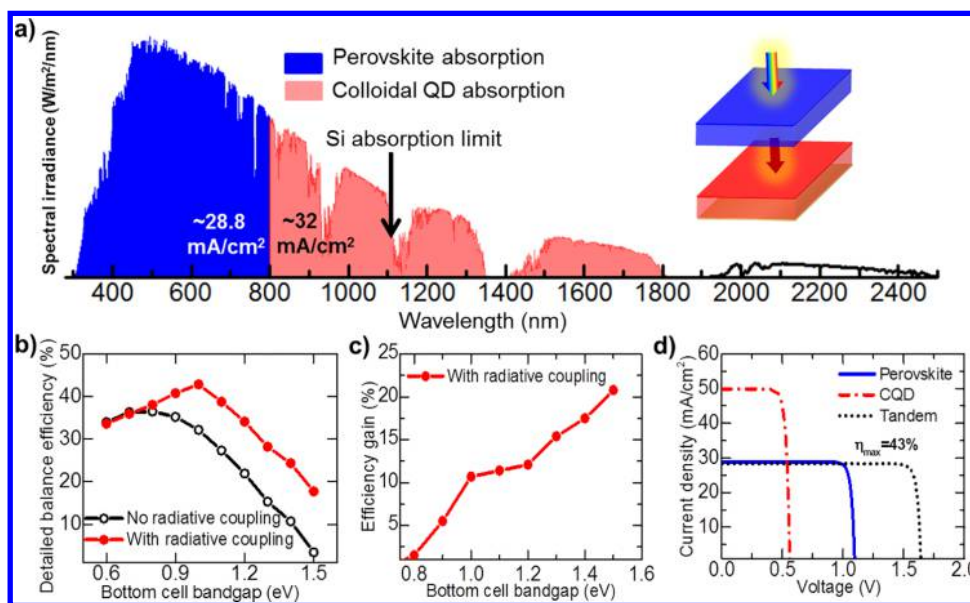
Figure 1. (a) Solar spectrum (AM1.5 global) showing the limit of photocurrent generation by a typical perovskite solar cell with a 1.55 eV bandgap and the lower-energy photons that could be captured by low-bandgap CQDs ($E_g \geq 0.65$ eV). (b) Theoretical detailed balance efficiency limits as functions of the CQD bottom-cell bandgap in a monolithic tandem cell configuration, with and without considering radiative coupling between subcells. The top cell is a typical perovskite cell with a bandgap of 1.55 eV (e.g., for $CH_3NH_3PbI_3$). The maximum achievable efficiency of 43% is obtained with an ideal CQD bottom-cell bandgap of 1.0 eV. The geometric factors assumed in these calculations are $(g_1, g_2, g_3, g_4) = (1,2,1,1)$ for the radiatively coupled tandems and $(0,2,0,1)$ for the tandems without radiative coupling (see eqs 1−4). (c) Efficiency gain ($\Delta\eta$) as a result of the radiative coupling between the top and bottom cells ($\Delta\eta = \eta_{RC} - \eta_0$, where η_{RC} and η_0 are the efficiency curves shown in (b)). (d) Theoretical $J-V$ curves derived from the detailed balance model for ideal individual and tandem cells.

extend the absorption edge further to harvest lower-energy photons (Figure 1a). Favorably, both CQD and perovskite material families are known to be highly luminescent.[26−31] We model below that the radiative coupling between the two subcell materials can critically influence the tandem cell performance. We also demonstrate an initial experimental realization of such a solar cell and model the performance of a tandem cell made from the highest-performing perovskite and CQD solar cells available.

The SQ detailed balance model (SQ model) for a single-junction solar cell assumes that (i) the cell absorbs radiation with photon energies higher than the bandgap from the sun or the surroundings and at the same time radiates to the surroundings (typically assumed to be a hemisphere); (ii) the absorption of each above-bandgap photon creates an electron−hole pair; apart from the generation of photocurrent, the only carrier relaxation process is radiative recombination emitting photons with energies above the bandgap; (iii) the sun and the surroundings are blackbody-like radiators, producing isotropic photon fluxes that can be described by a Planck distribution (or the standard AM1.5G spectrum for terrestrial solar cells); (iv) the active layer establishes a uniform chemical potential during operation to be in thermal equilibrium with the surroundings.[1,32] Extending these assumptions for a two-junction monolithic perovskite/CQD tandem solar cell, the current density (J) and voltage (V) generated by the tandem cell (J_{tandem}, V_{tandem}), the perovskite (J_{pero}, V_{pero}), and the CQD (J_{CQD}, V_{CQD}) subcells can be described by eqs 1−4.[32−36]

$$J_{tandem} = J_{pero} = J_{CQD} \tag{1}$$

$$V_{tandem} = V_{pero} + V_{CQD} \tag{2}$$

$$J_{pero} = \int_{E_{pero}}^{\infty} \Gamma(E)\, dE + g_1 \frac{2\pi q}{h^3 c^2} \int_{E_{pero}}^{\infty} \frac{E^2\, dE}{e^{\left(\frac{E - qV_{CQD}}{kT}\right)} - 1} - g_2 \frac{2\pi q}{h^3 c^2} \int_{E_{pero}}^{\infty} \frac{E^2\, dE}{e^{\left(\frac{E - qV_{pero}}{kT}\right)} - 1} \tag{3}$$

$$J_{CQD} = \int_{E_{CQD}}^{E_{pero}} \Gamma(E)\, dE + g_3 \frac{2\pi q}{h^3 c^2} \int_{E_{pero}}^{\infty} \frac{E^2\, dE}{e^{\left(\frac{E - qV_{pero}}{kT}\right)} - 1} - g_4 \frac{2\pi q}{h^3 c^2} \int_{E_{CQD}}^{\infty} \frac{E^2\, dE}{e^{\left(\frac{E - qV_{CQD}}{kT}\right)} - 1} \tag{4}$$

Here, E is the photon energy, E_{pero} and E_{CQD} are the bandgaps of perovskite and CQD cells, respectively, $\Gamma(E)$ is the energy-dependent distribution of photon flux based on the AM1.5G solar spectrum, q is the unit charge, h is the Planck constant, c is the speed of light, k is the Boltzmann constant, T is the ambient temperature (300 K), and g_1-g_4 are geometric factors that are influenced by the spatial power distribution of the radiation. For a simple monofacial planar radiator with isotropic radiation, the g value is 1. A planar bifacial isotropic radiator has a g value of 2.

Equation 1 describes the current matching condition in a monolithic tandem solar cell, where the two subcells are electrically connected in series. Equation 2 sets the condition for voltage addition of the subcells. In eq 3, the first term gives the photocurrent of the perovskite cell due to the solar irradiation. The second term calculates the additional photocurrent of the perovskite cell by recycling emission from the CQD cell. The third term describes the radiative recombination of the perovskite cell. Similarly, the first term in eq 4 considers
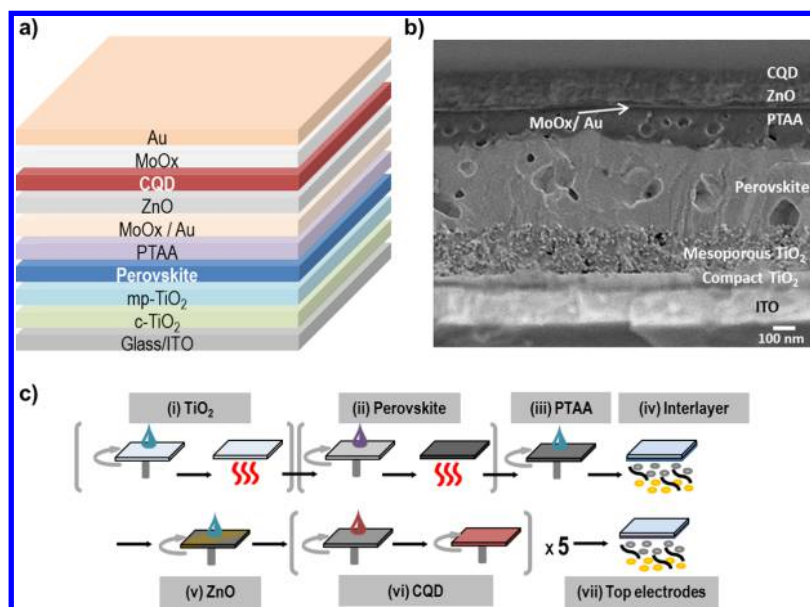
Figure 2. (a) Layer-by-layer device architecture of a monolithic perovskite/CQD tandem solar cell. The sunlight enters the solar cell from the glass substrate (superstrate) side, and the perovskite cell and the CQD cell are the top and bottom cells in the tandem structure, respectively. (b) Cross-sectional SEM image of the tandem cell. (c) Step-by-step device fabrication: (i) Compact and mesoporous TiO$_2$ deposition; (ii) perovskite deposition; (iii) PTAA deposition; (iv) MoO$_x$ and Au thermal evaporation; (v) ZnO deposition; (vi) QD film layer-by-layer deposition; (vii) MoO$_x$ and Au thermal evaporation.

the CQD photocurrent from the solar irradiation filtered by the perovskite top cell. The second term evaluates the additional CQD photocurrent contribution due to photon recycling from the perovskite cell. The third term describes the radiative recombination of the CQD cell.

As perovskites and CQDs are luminescent materials,[26−31] it is important to consider the radiative coupling between the two subcells while ensuring current matching for a monolithic tandem cell, as modeled in eqs 1−4. Recycling of emitted photons from solar cells is a strategy for enhancing the PCE.[37,38] Figure 1b shows the detailed balance limit, calculated for a two-junction solar cell with and without radiative coupling. A maximum efficiency of 43% has been obtained for a perovskite/PbS tandem cell system with radiative coupling between the top and the bottom cells and 37% without. It is interesting to note that the peak efficiencies occur at different bottom-cell bandgaps under two separate assumptions. While a 1 eV bottom-cell bandgap paired with the 1.55 eV perovskite top cell provides the best performance by assuming radiative coupling, 0.8 eV is the optimum bottom-cell bandgap without the coupling. This further emphasizes the importance of bandgap tunability of the bottom-cell material, and CQDs are very suitable for this purpose. Importantly, a significant contribution of radiative coupling to the tandem cell efficiencies is expected for CQD bottom-cell bandgaps of greater than 0.8 eV. The enhancement of PCE due to radiative coupling ranges from ∼11% for an optimum CQD bandgap of ∼1 eV to 20.8% for CQDs with a bandgap just below the perovskite bandgap. This efficiency gain is primarily due to the recycling of luminescence from the perovskite top cell by the CQD bottom cell. As the bandgap of the bottom cell approaches that of the top cell, the efficiency enhancement becomes more apparent as less energy is lost due to thermalization. In other tandem cell configurations where the top and the bottom cells are not closely connected as in a monolithic structure, the radiation from the top cell cannot be effectively coupled into the bottom

cell. This means that the >10% efficiency gain due to radiative coupling cannot be utilized in other systems.

As shown in Figure 1d, we have calculated the current−voltage (J−V) characteristics for individual cells using the SQ model and obtained a tandem cell J−V curve with an open-circuit voltage (V_{OC}) of 1.64 V and a short-circuit current (J_{SC}) of 28.4 mA/cm^2, leading to a 1-sun (AM1.5G) PCE of 43%.

We have designed and fabricated the first prototype of a solution-processable perovskite/CQD tandem solar cell, where the top perovskite unit cell absorbs the higher-energy photons and the bottom CQD cell absorbs in the near-IR region. The three main issues addressed in the design of such a multilayer monolithic architecture are (1) high-temperature annealing steps are avoided apart from the very first layer(s), to prevent thermal degradation of successive layers of materials; (2) ideal orthogonal solvents have been carefully selected for sequential deposition, to ensure intact underlying interfaces and layer thicknesses; and (3) a transparent recombination layer between the subcells has been designed, which also serves as a solvent barrier. Bearing these restrictions in mind, we choose a structure (Figure 2a) of ITO or FTO/compact titanium dioxide (TiO$_2$)/mesoporous TiO$_2$/CH$_3$NH$_3$PbI$_3$ perovskite/poly(bis(4-phenyl)(2,4,6-trimethylphenyl)amine (PTAA)/MoO$_x$/Au or Ag/zinc oxide (ZnO)/CQD/MoO$_x$/Au. From its cross-sectional SEM image (Figure 2b), it is evident that interfacial and layer integrity have been maintained by our processing sequence (Figure 2c). Starting with a substrate (superstrate) of ITO on glass, a layer of compact TiO$_2$ (50 nm) from a sol−gel solution in anhydrous ethanol and a layer of mesoporous TiO$_2$ (200 nm) diluted in ethanol are spin-coated under ambient atmosphere, each being annealed at 500 °C for 30 min after spin-coating. No subsequent thermal annealing above 100 °C is required. CH$_3$NH$_3$PbI$_3$ (280 nm) is spin-coated from a 0.6 M solution in anhydrous N,N-dimethylformamide, a polar aprotic solvent, and annealed at 100 °C for 45 min, followed by a layer of poly[bis(4-phenyl)(2,4,6-
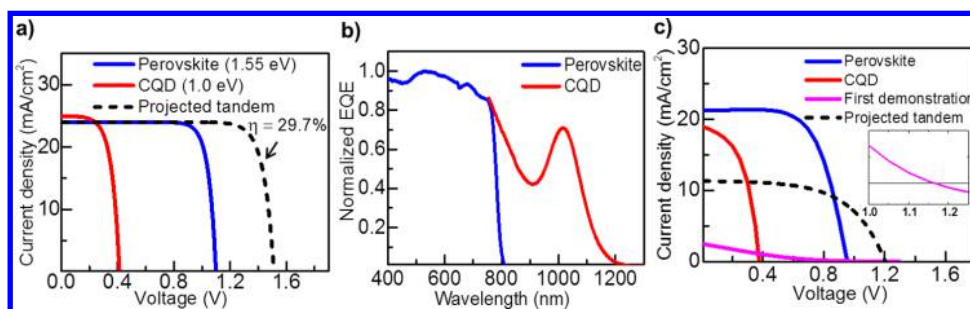
Figure 3. (a) CQD and perovskite $J-V$ curves and projected tandem cell performance based on state-of-the-art experimental results from ref 41 for a perovskite cell and from ref 42 for a CQD cell. The $J-V$ curve from ref 41 that uses CQDs with a 1.2 eV absorption cutoff was translated to the left by 0.2 eV to account for the reduced E_g of 1.0 eV, assuming that the $E_g - V_{OC}$ difference is not varying across the small range of bandgaps. The J_{SC} of the CQD subcell is estimated by considering only photons not absorbed by the perovskite cell (i.e., $E_{photon} < 1.55$ eV). A PCE of 29.7% is anticipated when combining the perovskite and CQD subcells in a tandem structure. (b) EQE spectra (normalized to unity) of individual cells used for the first demonstration of a monolithic tandem showing extended spectral response in the IR region using low-bandgap lead chalcogenide CQDs as the bottom-cell material. (c) Initial demonstration of voltage addition in the monolithic tandem structure, showing a V_{OC} of 1.17 V and a J_{SC} of 2.5 mA/cm^2 in a 1.55 eV perovskite/1.05 eV CQD tandem cell (pink curve). The black dotted curve shows a projected $J-V$ curve with a V_{OC} of 1.2 V and a J_{SC} of 11 mA/cm^2 with current matching, based on layer thickness optimization for the individual cells that we fabricated (blue curve for the perovskite cell and red curve for the CQD cell). The inset shows the V_{OC} of the first demonstration tandem cell (pink curve), indicating the intersection of the curve at zero current density.

trimethylphenyl)amine] (PTAA) (180 nm) spin-coated from the aromatic nonpolar toluene solution, both processed in a nitrogen-filled glovebox. The tunnel junction or interlayer consists of a thin bilayer of MoO$_x$ (7 nm) and Ag (0.5 nm) sequentially deposited by vacuum sublimation and a ZnO layer. The sublimation process does not disturb any underlying materials, and the sublimed bilayer can also serve as a solvent barrier for successive depositions. The ZnO layer is formed by spin-coating of ZnO nanocrystals in anhydrous isopropanol in ambient conditions, followed by annealing at 80−100 °C for 10−15 min. The solvent used does not dissolve the perovskite and PTAA layers underneath, and the annealing temperature does not cause degradation. No annealing steps are necessary hereafter. The ZnO nanocrystals used are synthesized according to the procedure described in ref 39 and are dispersed in isopropanol with moderate heating before use. The CQDs are deposited in a glovebox by the layer-by-layer solid-state ligand-exchange method adapted from the literature,[24,25,40] a process that involves anhydrous isopropanol (instead of the usual acetonitrile, which would dissolve and disintegrate the perovskite layer underneath) as solvent for the ligands (1,3-benzenedithiol and 1,2-ethanedithiol), and nonpolar octane for the CQDs. Finally, the stack is completed with vacuum-deposited MoO$_x$ (7 nm) and Au (80 nm) as the top electrode.

Combining our model with experimental data from the literature, we illustrate the tandem cell performance that can be expected in practice based on some of the highest-performing individual cells in Figure 3a. The blue curve in Figure 3a shows the $J-V$ characteristics of a 21.6% PCE perovskite solar cell ($E_g = 1.55$ eV).[41] The red curve shows $J-V$ characteristics of a PbS CQD solar cell,[42] with V_{OC} reduced to account for a lower bandgap of 1.0 eV and J_{SC} estimated by considering only photons not absorbed by the perovskite cell (i.e., $E_{photon} < 1.55$ eV). The black dotted curve, calculated by considering voltage addition and current matching of the subcells, indicates the postulated PCE for such a monolithic tandem device of 29.7%. Figure 3b presents the EQE profiles of the two individual cells to illustrate the spectral coverage of the tandem cell. Considering that the EQE of the tandem cell would generally follow the EQE profiles of the subcells, these profiles

demonstrate extended IR photon absorption beyond 1100 nm. In a fully optimized perovskite/CQD tandem cell, the extended IR response and EQE coverage are expected to outperform other solution-processed tandem solar cells and may find some applications in wide-bandwidth photodetectors.[43,44]

In Figure 3c, we present a preliminary experimental demonstration of the devices. On the basis of the empirical performance of the individual cells obtained in our laboratory—a 1.55 eV bandgap perovskite cell with reduced active layer thickness for current matching (blue curve) and a 1.03 eV bandgap PbS cell (red curve)—we anticipate a monolithic tandem cell to exhibit a V_{OC} of 1.20 V, J_{SC} of 11.33 mA/cm^2, fill factor (FF) of 0.57, and overall PCE of 7.8% (Figure 3c black dotted curve and Table 1) without considering any radiative coupling to give a conservative estimate. In the

Table 1. Experimental and Projected Solar Cell Characteristics under Standard AM1.5G Conditions[a]

device	V_{OC} (V)	J_{SC} (mA/cm^2)	FF	PCE (%)
thick perovskite	1.02	25.1	0.56	14.2
thin perovskite	0.95	21.2	0.64	13.0
CQD	0.38	19.0	0.50	3.6
tandem (thick perovskite)	1.31	0.11	0.20	0.03
tandem (thin perovskite)	0.98	5.0	0.20	1.01
projected monolithic tandem	1.20	11.3	0.57	7.8
projected monolithic tandem (SoA)	1.51	24	0.82	29.7

[a]"Thick perovskite" refers to a ~400 nm active layer, while "thin perovskite" has a thickness of ~280 nm. The CQD device was prepared using 1.21 eV PbS quantum dots. "Tandem (thick/thin perovskite)" refers to tandem devices fabricated with different perovskite thicknesses. "Projected monolithic tandem" is a semi-empirical tandem device projected from the experimental data of an individual 1.21 eV CQD cell and a 1.55 eV thin perovskite cell that we fabricated. "Projected monolithic tandem (SoA)" refers to a tandem device projected from the best state-of-the-art (SoA) CQD and perovskite solar cells from the literature. The experimental results were collected from about 200 devices, from which the best-performing devices were selected.

initial demonstration of the monolithic tandem devices, voltage addition has been observed, with a V_{OC} of 1.17 V (Figure 3c, pink curve) having been achieved from the integration of a "thin" perovskite cell with a V_{OC} of 0.95 V and a CQD cell with a V_{OC} of 0.38 V (Table 1, Figure 3c). Although a maximum V_{OC} of 1.31 V was achieved in the perovskite/CQD tandem structure (Table 1), we observed a trade-off between V_{OC} and J_{SC} during our layer thickness optimization experiments. The significant J_{SC} reduction of the tandem device with a thick perovskite top cell could be due to a combination of poor current matching and a nonideal tunnel junction. We acknowledge the technical challenges associated with the device engineering. In particular, the design and deposition of the tunnel junction need to be optimized. Given the thermal annealing and solvent polarity requirements in the sequential deposition, the types of materials available to choose from for the tunnel junction are limited. In principle, ZnO with another set of characteristics and processing conditions could lead to significant differences in material properties such as conductivity, charge extraction barriers, interfacial recombination rates, and morphology. Investigating the optimum combinations of material and processing conditions is a subject of further study. The existing difficulties currently limit the PCEs to 1.01% (Table 1) for the initial demonstration of perovskite/CQD monolithic tandem solar cells. In principle, overcoming the extrinsic technical limitations by utilizing a fully optimized structure could lead to an experimental PCE of up to 29.7% (Figure 3a).

In summary, we have proposed a perovskite/CQD tandem solar cell design that allows both bandgap tunability and solution processability. A detailed balance efficiency of 43% has been predicted for a perovskite (E_g = 1.55 eV)/CQD (E_g = 1.0 eV) tandem cell under standard AM1.5G solar illumination. An intersubcell radiative coupling effect recycles photons generated by radiative recombination, resulting in a significant enhancement (11−21% absolute gain) of the overall efficiency. For widely used high-performance perovskite absorbers with a bandgap of ~1.55 eV, the tandem structure has the potential to achieve high performance by harvesting near-IR photons. We have reported initial experimental results of a monolithic perovskite/CQD tandem solar cell, showing evidence of voltage addition of the top and bottom cells. SEM images show that our orthogonal solvent processing method is suitable for establishing the monolithic tandem structure. We expect that a 1-sun PCE of up to 29.7% is achievable by integrating state-of-the-art perovskite and CQD cells into the tandem cell design. The perovskite/CQD tandem structure may find further applications in broadband photodetectors.

■ AUTHOR INFORMATION

Corresponding Authors
*E-mail: dd403@cam.ac.uk (D.D.).
*E-mail: ncg11@cam.ac.uk (N.C.G.).
ORCID ⊙
Moritz H. Futscher: 0000-0001-8451-5009
Henry J. Snaith: 0000-0001-8511-790X
Neil C. Greenham: 0000-0002-2155-2432
Dawei Di: 0000-0003-0703-2809

Author Contributions
[#]A.K. and L.Y. contributed equally to the demonstration of the perovskite/CQD tandem solar cells. A.K. and D.D. developed the theoretical models of the tandem cells. S.B. synthesized the ZnO nanocrystals. M.H.F. helped with some ellipsometry measurements for optical modeling. A.K., L.Y., and D.D. wrote the initial manuscript. N.C.G. and B.E. provided useful suggestions. D.D. and L.Y. conceived the initial idea of the project. All authors contributed to the work. D.D. and N.C.G. planned the project and guided the work.

■ REFERENCES

(1) Shockley, W.; Queisser, H. J. Detailed Balance Limit of Efficiency of P-N Junction Solar Cells. *J. Appl. Phys.* **1961**, *32*, 510.

(2) Polman, A.; Knight, M.; Garnett, E. C.; Ehrler, B.; Sinke, W. C. Photovoltaic Materials: Present Efficiencies and Future Challenges. *Science* **2016**, *352*, 307.

(3) Green, M. A.; Bremner, S. P. Energy Conversion Approaches and Materials for High-Efficiency Photovoltaics. *Nat. Mater.* **2017**, *16*, 23−34.

(4) Green, M. A.; Hishikawa, Y.; Warta, W.; Dunlop, E. D.; Levi, D. H.; Hohl-Ebinger, J.; Ho-Baillie, A. W. H. Solar Cell Efficiency Tables (Version 50). *Prog. Photovoltaics* **2017**, *25*, 668−676.

(5) Chiu, P. T.; Law, D. C.; Woo, R. L.; Singer, S. B.; Bhusari, D.; Hong, W. D.; Zakaria, A.; Boisvert, J.; Mesropian, S.; King, R. R.; et al. 35.8% Space and 38.8% Terrestrial 5J Direct Bonded Cells. In *2014 IEEE 40th Photovoltaic Specialist Conference, PVSC 2014*; IEEE, Denver, CO, 2014; pp 11−13.

(6) Cariou, R.; Benick, J.; Beutel, P.; Razek, N.; Flotgen, C.; Hermle, M.; Lackner, D.; Glunz, S. W.; Bett, A. W.; Wimplinger, M.; et al. Monolithic Two-Terminal III-V//Si Triple-Junction Solar Cells with 30.2% Efficiency under 1-Sun AM1.5g. *IEEE J. Photovoltaics* **2017**, *7*, 367−373.

(7) Green, M. A.; Ho-Baillie, A.; Snaith, H. J. The Emergence of Perovskite Solar Cells. *Nat. Photonics* **2014**, *8*, 506−514.

(8) Park, N.-G.; Grätzel, M.; Miyasaka, T.; Zhu, K.; Emery, K. Towards Stable and Commercially Available Perovskite Solar Cells. *Nat. Energy* **2016**, *1*, 16152.

(9) Forgács, D.; Gil-Escrig, L.; Pérez-Del-Rey, D.; Momblona, C.; Werner, J.; Niesen, B.; Ballif, C.; Sessolo, M.; Bolink, H. J. Efficient Monolithic Perovskite/Perovskite Tandem Solar Cells. *Adv. Energy Mater.* **2017**, *7*, 1602121.

(10) Rajagopal, A.; Yang, Z.; Jo, S. B.; Braly, I. L.; Liang, P. W.; Hillhouse, H. W.; Jen, A. K. Y. Highly Efficient Perovskite−Perovskite Tandem Solar Cells Reaching 80% of the Theoretical Limit in Photovoltage. *Adv. Mater.* **2017**, *29*, 1702140.

(11) Eperon, G. E.; Hörantner, M. T.; Snaith, H. J. Metal Halide Perovskite Tandem and Multiple-Junction Photovoltaics. *Nat. Rev. Chem.* **2017**, *1*, 0095.

(12) Eperon, G. E.; Leijtens, T.; Bush, K. A.; Prasanna, R.; Green, T.; Wang, J. T. W.; McMeekin, D. P.; Volonakis, G.; Milot, R. L.; May, R.; et al. Perovskite-Perovskite Tandem Photovoltaics with Optimized Band Gaps. *Science* **2016**, *354*, 861−865.

(13) Chen, C.-C.; Bae, S.-H.; Chang, W.-H.; Hong, Z.; Li, G.; Chen, Q.; Zhou, H.; Yang, Y. Perovskite/Polymer Monolithic Hybrid Tandem Solar Cells Utilizing a Low-Temperature, Full Solution Process. *Mater. Horiz.* **2015**, *2*, 203−211.

(14) Noel, N. K.; Stranks, S. D.; Abate, A.; Wehrenfennig, C.; Guarnera, S.; Haghighirad, A.-A.; Sadhanala, A.; Eperon, G. E.; Pathak, S. K.; Johnston, M. B.; et al. Lead-Free Organic−Inorganic Tin Halide Perovskites for Photovoltaic Applications. *Energy Environ. Sci.* **2014**, *7*, 3061−3068.

(15) Zhao, B.; Abdi-Jalebi, M.; Tabachnyk, M.; Glass, H.; Kamboj, V. S.; Nie, W.; Pearson, A. J.; Puttisong, Y.; Gödel, K. C.; Beere, H. E.; et al. High Open-Circuit Voltages in Tin-Rich Low-Bandgap Perovskite-Based Planar Heterojunction Photovoltaics. *Adv. Mater.* **2017**, *29*, 1604744.

(16) Leijtens, T.; Prasanna, R.; Gold-Parker, A.; Toney, M. F.; McGehee, M. D. Mechanism of Tin Oxidation and Stabilization by Lead Substitution in Tin Halide Perovskites. *ACS Energy Lett.* **2017**, *2*, 2159−2165.

(17) Bush, K. A.; Palmstrom, A. F.; Yu, Z. J.; Boccard, M.; Cheacharoen, R.; Mailoa, J. P.; McMeekin, D. P.; Hoye, R. L. Z.; Bailie, C. D.; Leijtens, T.; et al. 23.6%-Efficient Monolithic Perovskite/Silicon Tandem Solar Cells with Improved Stability. *Nat. Energy* **2017**, *2*, 17009.

(18) Futscher, M. H.; Ehrler, B. Modeling the Performance Limitations and Prospects of Perovskite/Si Tandem Solar Cells under Realistic Operating Conditions. *ACS Energy Lett.* **2017**, *2*, 2089−2095.

(19) Futscher, M. H.; Ehrler, B. Efficiency Limit of Perovskite/Si Tandem Solar Cells. *ACS Energy Lett.* **2016**, *1*, 863−868.

(20) Li, M.; Gao, K.; Wan, X.; Zhang, Q.; Kan, B.; Xia, R.; Liu, F.; Yang, X.; Feng, H.; Ni, W.; et al. Solution-Processed Organic Tandem Solar Cells with Power Conversion Efficiencies > 12%. *Nat. Photonics* **2017**, *11*, 85−90.

(21) Xiao, Z.; Jia, X.; Ding, L. Ternary Organic Solar Cells Offer 14% Power Conversion Efficiency. *Sci. Bull.* **2017**, *62*, 1562−1564.

(22) Sargent, E. H. Colloidal Quantum Dot Solar Cells. *Nat. Photonics* **2012**, *6*, 133−135.

(23) Kim, G. H.; García De Arquer, F. P.; Yoon, Y. J.; Lan, X.; Liu, M.; Voznyy, O.; Yang, Z.; Fan, F.; Ip, A. H.; Kanjanaboos, P.; et al. High-Efficiency Colloidal Quantum Dot Photovoltaics via Robust Self-Assembled Monolayers. *Nano Lett.* **2015**, *15*, 7691−7696.

(24) Chuang, C.-H. M.; Brown, P. R.; Bulović, V.; Bawendi, M. G. Improved Performance and Stability in Quantum Dot Solar Cells through Band Alignment Engineering. *Nat. Mater.* **2014**, *13*, 796−801.

(25) Böhm, M. L.; Jellicoe, T. C.; Rivett, J. P. H.; Sadhanala, A.; Davis, N. J. L. K.; Morgenstern, F. S. F.; Gödel, K. C.; Govindasamy, J.; Benson, C. G. M.; Greenham, N. C.; et al. Size and Energy Level Tuning of Quantum Dot Solids via a Hybrid Ligand Complex. *J. Phys. Chem. Lett.* **2015**, *6*, 3510−3514.

(26) Yang, L.; Tabachnyk, M.; Bayliss, S. L.; Böhm, M. L.; Broch, K.; Greenham, N. C.; Friend, R. H.; Ehrler, B. Solution-Processable Singlet Fission Photovoltaic Devices. *Nano Lett.* **2015**, *15*, 354−358.

(27) Ning, Z.; Gong, X.; Comin, R.; Walters, G.; Fan, F.; Voznyy, O.; Yassitepe, E.; Buin, A.; Hoogland, S.; Sargent, E. H. Quantum-Dot-in-Perovskite Solids. *Nature* **2015**, *523*, 324−328.

(28) Di, D.; Musselman, K. P.; Li, G.; Sadhanala, A.; Ievskaya, Y.; Song, Q.; Tan, Z.-K.; Lai, M. L.; MacManus-Driscoll, J. L.; Greenham, N. C.; et al. Size-Dependent Photon Emission from Organometal Halide Perovskite Nanocrystals Embedded in an Organic Matrix. *J. Phys. Chem. Lett.* **2015**, *6*, 446−450.

(29) Cho, H.; Jeong, S. H.; Park, M. H.; Kim, Y. H.; Wolf, C.; Lee, C. L.; Heo, J. H.; Sadhanala, A.; Myoung, N. S.; Yoo, S.; et al. Overcoming the Electroluminescence Efficiency Limitations of Perovskite Light-Emitting Diodes. *Science* **2015**, *350*, 1222−1225.

(30) Dai, X.; Zhang, Z.; Jin, Y.; Niu, Y.; Cao, H.; Liang, X.; Chen, L.; Wang, J.; Peng, X. Solution-Processed, High-Performance Light-Emitting Diodes Based on Quantum Dots. *Nature* **2014**, *515*, 96−99.

(31) Ellingson, R. J.; Beard, M. C.; Johnson, J. C.; Yu, P.; Micic, O. I.; Nozik, A. J.; Shabaev, A.; Efros, A. L. Highly Efficient Multiple Exciton Generation in Colloidal PbSe and PbS Quantum Dots. *Nano Lett.* **2005**, *5*, 865−871.

(32) Shirasaki, Y.; Supran, G. J.; Bawendi, M. G.; Bulović, V. Emergence of Colloidal Quantum-Dot Light-Emitting Technologies. *Nat. Photonics* **2013**, *7*, 13−23.

(33) Nelson, J. Over the Limits: Strategies for High Efficiency. In *The Physics of Solar Cells*; Imperial College Press: London, 2003; pp 289−324.

(34) Brown, A. S.; Green, M. A. Limiting Efficiency for Current-Constrained Two-Terminal Tandem Cell Stacks. *Prog. Photovoltaics* **2002**, *10*, 299−307.

(35) Strandberg, R. Detailed Balance Analysis of Area De-Coupled Double Tandem Photovoltaic Modules. *Appl. Phys. Lett.* **2015**, *106*, 033902.

(36) De Vos, A. Detailed Balance Limit of the Efficiency of Tandem Solar Cells. *J. Phys. D: Appl. Phys.* **1980**, *13*, 839−846.

(37) Martí, A.; Araújo, G. L. Limiting Efficiencies for Photovoltaic Energy Conversion in Multigap Systems. *Sol. Energy Mater. Sol. Cells* **1996**, *43*, 203−222.

(38) Pazos-Outon, L. M.; Szumilo, M.; Lamboll, R.; Richter, J. M.; Crespo-Quesada, M.; Abdi-Jalebi, M.; Beeson, H. J.; Vru ini, M.; Alsari, M.; Snaith, H. J.; et al. Photon Recycling in Lead Iodide Perovskite Solar Cells. *Science* **2016**, *351*, 1430−1433.

(39) Bai, S.; Wu, Z.; Wu, X.; Jin, Y.; Zhao, N.; Chen, Z.; Mei, Q.; Wang, X.; Ye, Z.; Song, T.; et al. High-Performance Planar Heterojunction Perovskite Solar Cells: Preserving Long Charge Carrier Diffusion Lengths and Interfacial Engineering. *Nano Res.* **2014**, *7*, 1749−1758.

(40) Lan, D.; Geisz, J. F.; Steiner, M. A.; Garcia, I.; Friedman, D. J.; Green, M. A. Improved Modeling of Photoluminescent and Electroluminescent Coupling in Multijunction Solar Cells. *Sol. Energy Mater. Sol. Cells* **2015**, *143*, 48−51.

(41) Yang, W. S.; Park, B. W.; Jung, E. H.; Jeon, N. J.; Kim, Y. C.; Lee, D. U.; Shin, S. S.; Seo, J.; Kim, E. K.; Noh, J. H.; et al. Iodide Management in Formamidinium-Lead-Halide-Based Perovskite Layers for Efficient Solar Cells. *Science* **2017**, *356*, 1376−1379.

(42) Lan, X.; Voznyy, O.; García De Arquer, F. P.; Liu, M.; Xu, J.; Proppe, A. H.; Walters, G.; Fan, F.; Tan, H.; Liu, M.; et al. 10.6% Certified Colloidal Quantum Dot Solar Cells via Solvent-Polarity-Engineered Halide Passivation. *Nano Lett.* **2016**, *16*, 4630−4634.

(43) García De Arquer, F. P.; Armin, A.; Meredith, P.; Sargent, E. H. Solution-Processed Semiconductors for Next-Generation Photodetectors. *Nature Reviews Materials* **2017**, *2*, 16100.

(44) Dhanabalan, S. C.; Ponraj, J. S.; Zhang, H.; Bao, Q. Present Perspectives of Broadband Photodetectors Based on Nanobelts, Nanoribbons, Nanosheets and the Emerging 2D Materials. *Nanoscale* **2016**, *8*, 6410−6434.